Lab on a Chip

PAPER

View Article Online
View Journal | View Issue

Cite this: *Lab Chip*, 2026, **26**, 2295

Integrated strategy for breast cancer biomarker analysis using dual ionic liquid aqueous biphasic systems and microfluidic immunoassays

Maria S. M. Mendes,[ab] Inês Agostinho,[bc] Maria C. Souza,[a] Virginia Chu,[b] Mara G. Freire,[a] Francisca A. e Silva *[a] and João P. Conde*[bc]

Human epidermal growth factor receptor 2 (HER2) is a key biomarker in breast cancer diagnosis, prognosis, and therapeutic decision-making. While its determination is traditionally based on tissue biopsy, serum-based testing is a simpler and less invasive alternative. However, its implementation remains challenging due to matrix effects and interference from high-abundance proteins, leading to insufficient sensitivity and specificity. To overcome these limitations, this work reports the development and optimization of a novel microfluidic immunoassay for HER2 detection in human serum, incorporating an innovative sample pretreatment step using a dual ionic liquid aqueous biphasic system (IL–IL-ABS). Under optimized conditions, the ABS composed of tri(isobutyl)methylphosphonium tosylate ($[P_{i(444)1}][TsO]$) and cholinium dihydrogenphosphate ($[Ch][H_2PO_4]$) effectively depleted high-abundance proteins (up to 100% removal) while selectively extracting 97% of HER2 into a separate aqueous phase. HER2 detection was performed in a protein G bead-based microfluidic device, demonstrating robust performance across diverse matrices. The limit of detection in ABS-pretreated serum (14.06 ng mL^{-1}) was significantly improved compared to direct serum analysis (24.33 ng mL^{-1}) and PBS (18.99 ng mL^{-1}). By integrating advanced sample pretreatment with a sensitive microfluidic immunoassay, this work enhances the accuracy of HER2 quantification in complex biological samples, offering a promising approach for improved breast cancer detection and point-of-care applications.

Received 30th October 2025,
Accepted 25th February 2026

DOI: 10.1039/d5lc01010a

rsc.li/loc

Introduction

Based on the latest global cancer survey, breast cancer ranks as the second most frequently diagnosed and deadliest form of cancer.[1,2] Clinical biomarkers such as oestrogen receptor (ER), progesterone receptor (PR), and human epidermal growth factor receptor 2 (HER2) play an increasingly important role in early diagnosis, effective prognosis and treatment selection.[3] *Circa* of 10–30% of breast cancers occur with amplification and/or overexpression of HER2 gene located on chromosome 17q12.[4] Current techniques to evaluate HER2 status include the assessment of protein overexpression using immunohistochemistry (IHC) or the evaluation of gene amplification resorting to fluorescent *in situ* hybridization (FISH).[5] Although highly reliable, such techniques are time-, labour- and resource-intensive, requiring highly qualified professionals to carry out complex and invasive procedures.[6,7] In contrast, HER2 serum-based testing has been highlighted as a simpler approach, avoiding invasive tissue biopsies and allowing repeated biomarker monitoring over time.[8,9] HER2-positive breast cancer patients typically exhibit circulating HER2 levels higher than 15 ng mL^{-1}, which require techniques able to precisely quantify such low concentrations.[10,11] The most frequently employed technique for HER2 quantification is enzyme-linked immunosorbent assay (ELISA).[12] However, ELISA involves complex, multi-stage protocols that typically require trained personnel, and costly, specialized reagents and equipment.[2]

Microfluidic lab-on-a-chip devices have emerged as cost-effective and accurate alternatives for biomarker detection, enabling miniaturization, automation, faster response times, and lower sample and reagent consumption than traditional laboratory techniques.[13,14] Such features render them particularly well-suited for point-of-care (PoC) diagnostics, while also enhancing the capacity for HER2 detection in both clinical and resource-constrained environments.[13] A variety of microfluidic platforms has been developed for HER2 detection, employing transduction mechanisms such as electrochemical, optical, and piezoelectric sensing.[15–17]

[a] *CICECO – Aveiro Institute of Materials, Department of Chemistry, University of Aveiro, Aveiro, Portugal. E-mail: francisca.silva@ua.pt*
[b] *Instituto de Engenharia de Sistemas e Computadores – Microsistemas e Nanotecnologias (INESC MN), Lisbon, Portugal*
[c] *Department of Bioengineering, Instituto Superior Técnico, Universidade de Lisboa, Lisbon, Portugal. E-mail: joao.conde@tecnico.ulisboa.pt*

Among these, electrochemical microfluidic systems have achieved high sensitivity, with limits of detection reaching the picogram per millilitre and even femtomolar range in serum samples.[15,18] For instance, devices incorporating screen-printed carbon electrodes, gold nanoparticles, and enzyme labels have facilitated rapid and sensitive HER2 quantification.[18–20] Optical microfluidic biosensors, including opto-fluidic ring resonators and surface plasmon resonance systems, also offer label-free, real-time detection capabilities suitable for clinical monitoring.[17] Despite these advances, many of these technologies remain at the proof-of-concept stage. Key challenges, such as sensor stability, the need for efficient sample preparation, and interference from complex biological matrices, continue to hinder their clinical translation. To fully harness the potential of these platforms, continued innovation in system integration, surface functionalization, and signal amplification is essential.

The complex medium of human serum and the broad concentration range of serum proteins create interferences in serum-based testing that impose a significant challenge in the reliable quantification of low-abundance biomarkers, particularly at the PoC.[21] Human serum albumin (HSA) stands as the most abundant protein in serum, representing approximately 55–60% of the proteomic content, followed by immunoglobulin G (IgG) that comprises around 10–20% of the total protein content.[22] Together with other relatively abundant proteins, such as transferrin, haptoglobin, and α1-antitrypsin, these components are estimated to represent up to ~90% of the total serum proteome.[23] The implementation of a sample pretreatment step to remove high-abundance proteins effectively reduces the complexity of serum, thereby minimizing their capacity to interfere with or mask the detection of low-abundance biomarkers.[24]

Common strategies for high-abundance protein removal and biomarker extraction include precipitation using salting-out agents, polymers or organic solvents, as well as affinity enrichment or depletion using columns with specific ligands for targeting proteins.[25] However, these strategies have inherent limitations that constrain their clinical applicability and can lead to false positive or false negative results. Such limitations are dependent on the technique and may include incomplete removal of high-abundance proteins, lack of specificity in targeting these proteins, potential impacts on the integrity and stability of biomarkers, frequent biomarker losses, multi-step procedures, reliance on volatile organic solvents or expensive resources and limited miniaturization potential.[25] Hence, there remains a need for the development of a method that can efficiently mitigate matrix effects, while also addressing technological, environmental and economic concerns, especially at the PoC.[26]

Aqueous biphasic systems (ABS), typically formed by polymers, high-melting salts, or surfactants, are biomarker-friendly, all-aqueous alternative liquid–liquid extraction approaches, suitable for bioanalytical sample pretreatment.[27] Earlier research has demonstrated that polymer–polymer-ABS can separate alkaline phosphatase isoforms from bile, serum and placenta, with selective separation occurring only when one of the polymers is functionalized with a hydrophobic ligand.[28] Surfactant-based systems have been used to remove albumin from human biological samples, such as serum, prior to bioanalysis using laboratory-based techniques, though with modest efficiency.[29] For removing both IgG and HSA, polymer–salt-ABS have also shown potential for lung cancer serum-based detection.[30] Despite such progress, conventional ABS still face limited polarity range, which hinders the applicability in clinical settings and PoC detection, where an optimal balance between selectivity and efficiency is a critical requirement.[31]

Ionic liquids (ILs) are highly structurally versatile compounds, which grant access to a diverse library of ABS components simply by tuning their ionic pairings. These can be combined with strong salting-out agents or polymers to form ABS, providing a more customizable spectrum of interactions and affinities during sample pretreatment, which in turn enhances selective extraction.[29,32,33] These IL–ABS attributes were underscored in a recent study for the simultaneous depletion of IgG and HSA while extracting prostate specific antigen (PSA), a prostate cancer biomarker, from human serum.[34] Using ILs in ABS formation allowed for the customization of the sample pretreatment process, enhancing biomarker extraction yield.[34] Furthermore, these systems were used prior PSA detection *via* a microfluidic immunoassay.[35] However, the most efficient removal of high-abundance proteins was achieved with ABS formed by an IL and a strong salting-out agent, which also caused co-precipitation of PSA (about 28%).[34] A more balanced ability to deplete high-abundance serum proteins while preserving biomarkers is crucial, particularly in clinical and PoC settings, where biomarker loss can negatively affect patient care.

To overcome these limitations, this work introduces an innovative sample pretreatment strategy based on dual IL-ABS (IL–IL-ABS), replacing the conventional single IL approach. This strategy enables broader polarity modulation by extending the tailoring capacity to both phases of the ABS, in contrast to traditional IL–salt and IL–polymer systems, where tunability is confined to a single phase. The goal is to develop a more efficient and selective pretreatment method for human serum samples, with IL–IL-ABS evaluated for their ability to simultaneously deplete high-abundance proteins and extract HER2 prior to analysis and compared against conventional ABS configurations. Furthermore, to fully unlock the potential of HER2 as an accessible biomarker and overcome the constraints of serum-based testing at the PoC, the advantages of IL–IL-ABS were integrated with microfluidic devices. For the first time, the feasibility of HER2 detection in serum by immunofluorescence within a microfluidic device is demonstrated following sample pretreatment using an IL–IL-ABS.

Materials and methods

Phase-forming components, biological samples, and analytical reagents

Several phase-forming components were combined to prepare ABS, as illustrated in Fig. 1, particularly in Fig. 1A. Tetrabutylphosphonium bromide ($[P_{4444}]Br$, purity of 95 wt%) and tetrabutylphosphonium chloride ($[P_{4444}]Cl$, purity of 95 wt%) were acquired from Iolitec, while tri(isobutyl) methylphosphonium tosylate ($[P_{i(444)1}][TsO]$, purity >95 wt%), tri(butyl)methylphosphonium methylsulfate ($[P_{4441}][CH_3SO_4]$, purity >96 wt%) and ethyl(tributyl)phosphonium diethylphosphate ($[P_{4442}][Et_2PO_4]$, purity of 95 wt%) were supplied by CYTEC. Cholinium dihydrogen phosphate ([Ch] $[H_2PO_4]$, purity >98 wt%) and cholinium acetate ([Ch][CH_3COO], purity >99 wt%) were acquired from Iolitec. The chemical structures and corresponding abbreviations of the ILs are depicted in Fig. 1B. Polypropylene glycol with an average molecular weight of 400 g mol^{-1} (PPG 400) was obtained from Sigma-Aldrich. Potassium citrate tribasic monohydrate ($K_3C_6H_5O_7{\cdot}H_2O$, purity ≥99 wt%) from Acros Organics and citric acid ($C_6H_8O_7{\cdot}H_2O$, purity ≥99.5 wt%) from Panreac were used to prepare a citrate buffered salt solution at pH ≈ 7. Phosphate-buffered saline (PBS, pH ≈ 7.4) was prepared using pellets from Sigma-Aldrich according to manufacturer instructions.

As the complex biological sample, human serum (H4522, Lot #SLCD4040) was commercially obtained from Sigma-Aldrich. Serum protein standards used were purified human IgG solution (29.4 mg mL^{-1}), sourced from Innovative Research, Inc., and lyophilized human albumin powder (purity ≥96%), from Alfa Aesar. ERBB2/HER2 ELISA kit (RAB0173-1KT Lot #0106I287) was acquired from Sigma-Aldrich.

HPLC buffer was prepared using sodium dihydrogen phosphate monohydrate ($NaH_2PO_4{\cdot}H_2O$, purity of 99 wt%) and disodium hydrogen phosphate heptahydrate ($Na_2HPO_4{\cdot}7H_2O$, purity of 99 wt%) from Panreac, and sodium chloride (NaCl, extra pure) from Fisher Scientific. Water was purified through double distillation, reverse osmosis, and treatment with a Milli-Q plus 185 apparatus.

For the microfluidic immunoassay development, protein G Sepharose® 4 Fast Flow microbeads were acquired from Cytiva. Recombinant human ERbB2/HER2 protein

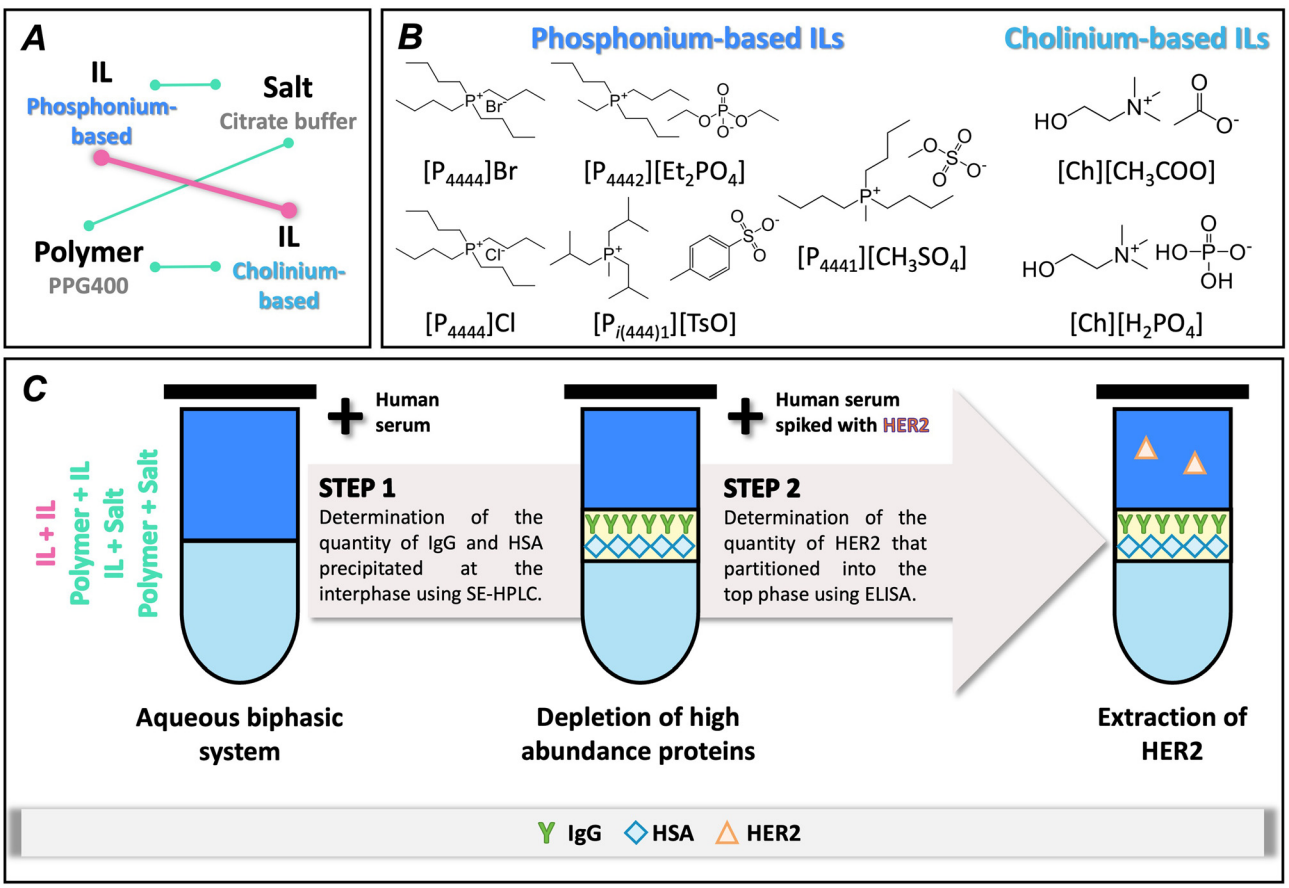

Fig. 1 Technical considerations for the design of IL–IL-ABS as sample pretreatment strategies. (A) Combinations of different types of phase-forming components used to generate ABS, including dual ILs and conventional components. (B) Chemical structures and corresponding abbreviations of the ILs employed. (C) Experimental workflow implemented to evaluate the depletion of high-abundance serum proteins and the extraction of HER2.

(ab168896), anti-ErbB2/HER2 capture antibody (ab281274), and anti-ErbB2/HER2 detection antibody (ab281124) were sourced from Abcam. Alexa Fluor® 430 NHS ester for antibody labelling was acquired from ThermoFisher Scientific.

Evaluation of high-abundance serum protein depletion in ABS

Two sets of IL–IL-ABS were investigated: one fixing [Ch][H_2PO_4], while varying the phosphonium-based IL ([P_{4444}]Br, [P_{4444}]Cl, [$P_{i(444)1}$][TsO], [P_{4441}][CH_3SO_4], and [P_{4442}][Et_2PO_4]; other sharing [P_{4444}]Br as the common IL, while changing the cholinium-based IL ([Ch][H_2PO_4] and [Ch][CH_3COO]). Conventional ABS composed of PPG 400 + $K_3C_6H_5O_7$/$C_6H_8O_7$, PPG 400 + [Ch][H_2PO_4], and [$P_{i(444)1}$][TsO] + $K_3C_6H_5O_7$/$C_6H_8O_7$ were also evaluated for comparative purposes.

A fixed biphasic mixture was selected for most systems, each with a final mass of 1 g: 30 wt% phosphonium-based IL or PPG 400, 35 wt% cholinium-based IL or $K_3C_6H_5O_7$/$C_6H_8O_7$, 33 wt% PBS and 2 wt% human serum. An exception was the [P_{4442}][Et_2PO_4] + [Ch][H_2PO_4] system, for which the mixture composition studied was 40 wt% [P_{4442}][Et_2PO_4], 35 wt% [Ch][H_2PO_4], 23 wt% PBS and 2 wt% human serum, due to its narrower operational window for ABS formation. Furthermore, for the ABS composed of 30 wt% [$P_{i(444)1}$][TsO] and 35 wt% [Ch][H_2PO_4] was further evaluated with 5 wt% and 10 wt% serum to assess the effect of sample amount. In all cases, the PBS content was adjusted accordingly to complete the system composition to 100 wt%. Triplicates of each ABS were prepared by accurately weighing the appropriate quantities of each component, enabling the determination of average values and their respective standard deviations. Then, the mixtures were thoroughly stirred in a vortex and centrifuged during 10 minutes at 3500 rpm. Subsequently, the top and bottom phases were carefully collected using syringes.

IgG and HSA were selected as representative high-abundance proteins because: (i) together they account for more than 80% of the total proteomic content of human serum;[22] (ii) they are the dominant contributors to matrix effects in bioanalytical assays;[24] and (iii) they are readily detectable in the serum chromatographic profile. Other moderate- and low-abundance proteins are also present in serum but are not directly detectable under the applied HPLC conditions.[23] Therefore, any improvements in microfluidic assay performance observed after ABS pretreatment are discussed in terms of IgG and HSA depletion.

Quantification of IgG and HSA in the top and bottom phases was performed by diluting 100 μL aliquots of each phase in 900 μL of HPLC buffer and analysing them by HPLC. The amount of IgG and HSA precipitated at the interphase was determined through mass balance to the initial amount added to each ABS. Considering the thin, fragile interphase formed in these systems, which limits its physical isolation, this approach provides a reliable quantitative assessment and is commonly applied in our previous ABS-based protein separation studies.[30,34] Potential interferences from the ABS phase-forming components were considered, and blank controls were prepared by adding water instead of human serum in each ABS. Standards with concentrations ranging from 0.01 to 1.0 mg mL^{-1} were analysed for the establishment of calibration curves for IgG and HSA.

Chromatographic analyses were conducted using a Chromaster HPLC system (VWR Hitachi), featuring a binary pump, a column oven set at 25 °C, an auto-sampler maintained at 10 °C and a diode array detector (DAD), with separation achieved using a Shodex Protein KW-802.5 column (8 mm × 300 mm). An isocratic elution was performed using 50 mM sodium phosphate buffer (NaH_2PO_4/Na_2HPO_4) with 0.3 M NaCl as the mobile phase, at a flow rate of 0.5 mL min^{-1} over a 40 min-run. Analyses were performed with a 25 μL injection volume and detection at 280 nm. Under these analytical conditions, IgG and HSA exhibited retention times of approximately 15 minutes and 16 minutes, respectively.

The depletion efficiencies of IgG and HSA ($DE_{IgG/HSA}$, %) were determined to evaluate the capability of ABS to precipitate high-abundance proteins at the solid interphase, according to the following equation:

$$DE_{IgG/HSA}\% = \frac{w^{Inter}_{IgG/HSA}}{w^{Serum}_{IgG/HSA}} \times 100 \quad (1)$$

where $w^{Inter}_{IgG/HSA}$, and $w^{Serum}_{IgG/HSA}$ represent the mass of IgG and HSA in the interphase and their initial mass in the serum sample, respectively. The same equation was applied to calculate the recovery yields of IgG and HSA ($RY_{IgG/HSA}$, %) to the liquid phases, replacing the mass of protein in the interphase with the corresponding mass in either the top or bottom phase.

Assessment of HER2 partition and extraction in ABS

The most efficient IL–IL-ABS were then evaluated in terms of their performance to extract HER2 from serum in one of the aqueous phases: [P_{4444}]Br + [Ch][H_2PO_4], [P_{4444}]Br + [Ch][CH_3-COO], [$P_{i(444)1}$][TsO] + [Ch][H_2PO_4], and [P_{4441}][CH_3SO_4] + [Ch][H_2PO_4] as well as the conventional ABS composed of PPG 400 + $K_3C_6H_5O_7$/$C_6H_8O_7$, PPG 400 + [Ch][H_2PO_4], and [$P_{i(444)1}$][TsO] + $K_3C_6H_5O_7$/$C_6H_8O_7$. Similar preparation and separation procedures were applied as described earlier.

Preliminary assessments were performed to study the partition of HER2 in ABS in the absence of human serum by using an aqueous solution of the biomarker at 15 ng mL^{-1}, which corresponds to clinically relevant levels.[36] In experiments involving human serum, all samples were spiked with the target analyte at an identical concentration. The HER2 content in the top and bottom phases was determined using ELISA kits following the manufacturer's validated protocol and using a calibration curve ranging from 8.19 pg mL^{-1} to 2000 pg mL^{-1}. When an interphase was formed, the HER2 content in this phase was estimated by mass balance,

based on the initial concentration of HER2 in the sample. Blank ABS were also prepared to address possible interferences of ABS phase-forming components. This procedure yields precise and reproducible measurements, with standard deviations below 10%, which is within the manufacturer-specified error range of the ELISA kit.

The recovery yield of HER2 (RY_{HER2}, %) in the top, inter and bottom phases of the different ABS containing either the HER2 aqueous solution or HER2 spiked human serum was calculated using the following equation:

$$RY_{HER2}\% = \frac{w_{HER2}^{Top/Inter/Bottom}}{w_{HER2}^{Initial}} \times 100 \quad (2)$$

where w_{HER2}^{Top}, w_{HER2}^{Inter} and w_{HER2}^{Bottom} correspond to the mass of HER2 in the top phase, in the interphase, and in the bottom phase, respectively, and $w_{HER2}^{Initial}$ represents the total mass of HER2 in the initial mixture.

Fig. 1C provides an overview of the experimental strategy adopted in this work for the development and optimization of the IL–IL-ABS pretreatment, comprising two sequential and complementary evaluation steps. The first consisted of an initial screening using human serum to assess the performance of different ABS for the depletion of high-abundance proteins, while the second applied the most promising ABS identified in the first step to achieve simultaneous depletion and HER2 extraction from spiked human serum.

Microfluidic structures fabrication, fluids handling and image acquisition

Fig. 2 depicts the microfluidic device for HER2 detection, following a previously reported bead-based immunoassay approach in which height-based constrictions are employed to secure beads reliably within the channel.[37] The dual-channel structure, with heights of 20 μm and 100 μm, forms a packed bed that efficiently retains protein G microbeads (diameter ~90 μm) at the interface. Beads are introduced through a larger inlet chamber, which is subsequently sealed with a plug (Fig. 2A), while the smaller chamber hosts the immunoassay, with dedicated inlets and outlets for reagent flow (Fig. 2B). This configuration allows precise control of assay conditions, minimizes signal gradients, and ensures efficient antibody–antigen interactions for reproducible fluorescence-based detection.

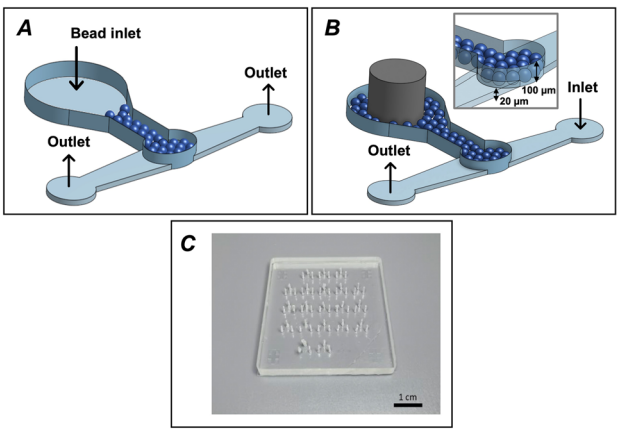

Fig. 2 Microfluidic device designed for HER2 detection. The device features two microchannels with distinct heights: a shallower channel with a height of 20 μm and a taller chamber with a height of 100 μm. (A) Fluidic handling for microbeads packing. (B) Fluidic handling for experiment performance in which the bead inlet is closed using a metallic plug. (C) Fabricated PDMS microfluidic chip. Adapted from ref. 37 under the terms of the Creative Commons CC-BY license.

To convert this design into an operational device, microfluidic structures were fabricated by soft lithography using polydimethylsiloxane (PDMS; Sylgard 184 elastomer kit, Dow Corning, Midland, MI, USA), following a previously reported three-step procedure:[38] (i) aluminium hard mask fabrication, (ii) SU-8 mould production, and (iii) PDMS casting. Hard masks of patterned aluminium on glass were fabricated with optical lithography and patterned by wet chemical etching. To include an enclosed chamber for microbead trapping, two hard masks were necessary to produce a two-level microfluidic column. For the SU-8 mould production, a 20 μm thick SU-82015 layer (Microchem Corp., Newton, MA, USA) was spin-coated onto a clean silicon substrate (University Wafer, South Boston, MA, USA) and baked at 95 °C for 4 minutes. The aluminium mask for the 20 μm design was aligned over the substrate, exposed to UV light, and subjected to a second baking cycle at 95 °C for 5 minutes. The mould was developed by immersion in propylene glycol monomethyl ether acetate (PGMEA), followed by rinsing with isopropyl alcohol (IPA) and drying. A second layer of 100 μm thick was applied on top of the first using the SU-8 50 negative photoresist (Microchem Corp., Newton, MA, USA), baked at 65 °C for 10 minutes and at 95 °C for 30 minutes. The second aluminium mask for the 100 μm design was aligned with the first layer, exposed to UV light, and subjected to a post-exposure bake at 65 °C for 1 minute and at 95 °C for 10 minutes. After development in PGMEA and rinsing with IPA, a final bake at 150 °C for 15 minutes was performed. For the casting of the PDMS structures, a mixture of PDMS elastomer in a 10 : 1 ratio of base to curing agent was prepared, degassed to remove air bubbles, poured over the mould, and cured by baking at 70 °C for 1.5 hours. After curing, the PDMS structures were carefully peeled off the mould and access holes were punched for the outlets and inlets. The structures were then sealed into a 500 μm thick PDMS membrane using an oxygen plasma cleaner (Harrick Plasma, Ithaca, NY, USA) to ensure a strong irreversible bond. The final PDMS chip consisted of an array of 20 microchannel devices with two sections, as presented in Fig. 2C.

For fluid handling, a NE-1002X syringe pump (New Era Pump Systems, Inc., Nassau, NY, USA) was used to precisely control fluid flow. 1 mL syringes (U-100 CODAN, Lensahn, Germany) were installed in the pump and connected to a 20-gauge luer stub adapter, which was then linked to a

polyethylene BTPE-60 tube (Instech Laboratories, Inc., PA, USA). To connect the BTPE-60 tube to the microchannel outlet, an open metallic adapter (Instech Laboratories, Inc., Montgomery, PA, USA) was employed. Fluids within the microchannel were manipulated by generating negative pressure through the syringe pump, effectively drawing the solution from the inlet to the outlet.

For image acquisition, a Leica DMLM fluorescence microscope equipped with a Leica DFC300FX digital camera was used. To detect Alexa 430-labeled molecules, a blue light filter with an excitation range of 450–490 nm was employed. Images were captured with a 1 second exposure time, 10× magnification, and 1× gain. Fluorescence intensity was quantified using ImageJ software (National Institutes of Health, USA), determining intensity values by calculating the difference between the mean intensity within the channel and the background intensity outside the channel, based on two independent experiments.

Microfluidic sandwich immunoassay

The microfluidic sandwich immunoassay for HER2 detection was conducted using a systematic approach to ensure sensitivity and specificity. Initially, protein G microbeads were packed into the microchannel at a flow rate of 8 μL min^{-1} for 3 minutes, followed by a washing step with PBS at the same flow rate for an additional 3 minutes. Subsequently, a 100 μg mL^{-1} solution of capture anti-HER2 antibody was introduced into the channel at a flow rate of 0.5 μL min^{-1} for 10 minutes to immobilize the antibodies on the beads. After immobilization, a blocking step was performed by introducing a 1 mg mL^{-1} IgG solution at the same flow rate for 10 minutes to minimize non-specific binding. To detect HER2, solutions spiked with HER2 at concentrations ranging from 5 to 25 ng mL^{-1} were introduced into the microchannel at a flow rate of 0.5 μL min^{-1} for 10 minutes. Negative controls containing 0 ng mL^{-1} HER2 were included for each condition to establish baseline measurements. Following the introduction of the HER2 samples, a 100 μg mL^{-1} solution of detection anti-HER2 antibody labelled with Alexa 430 was pumped into the channel at 0.5 μL min^{-1} for 10 minutes to facilitate the detection of HER2. Between each assay step, PBS was flowed through the microchannel at a flow rate of 5 μL min^{-1} for 1 minute to remove any unbound molecules and reduce background noise.

To calculate the sensitivity curves and limits of detection (LoDs) for HER2, a quantitative approach was employed using fluorescence intensity measurements obtained from the microfluidic sandwich immunoassay. For each sample matrix, HER2 concentrations ranging from 5 to 25 ng mL^{-1} were tested, and fluorescence intensities were quantified. The sensitivity curves were generated by plotting fluorescence intensity against HER2 concentration for each condition, including HER2 in PBS, untreated human serum, spiked in the top phase of the ABS containing 30 wt% $[P_{i(444)1}][TsO]$, 35 wt% $[Ch][H_2PO_4]$ and 35 wt% PBS (without serum), and HER2 in the top phase of the ABS containing 30 wt% $[P_{i(444)1}][TsO]$, 35 wt% $[Ch][H_2PO_4]$, 25 wt% PBS and 10 wt% serum spiked with HER2 after serum pretreatment. The LoD for each condition was determined by calculating the concentration at which the fluorescence signal was three standard deviations above the baseline signal obtained from the negative control (0 ng mL^{-1} HER2). The relative standard deviations (RSD, %) were calculated for each concentration as the standard deviation of replicate measurements divided by their mean, multiplied by 100, and are reported as a concentration-dependent range.

Results and discussion

IL–IL-ABS for protein depletion and HER2 extraction

To form the IL–IL-ABS, various combinations of phosphonium-based and cholinium-based ILs were investigated, given their enhanced tunability across both phases. In these systems, the phosphonium-based IL acts as a salting-in species, while the cholinium-based IL acts as the salting-out agent, generating an aqueous incompatibility that leads to phase separation. This initial screening helped elucidate the influence of IL structure on the depletion of high-abundance proteins (IgG and HSA) and the extraction of HER2. Fig. 3 shows the depletion efficiencies obtained for IgG and HSA. Detailed data on depletion efficiencies are provided in the SI, along with the recovery yields of IgG and HSA obtained for the top and bottom phases (Table S1).

IL–IL-ABS comprising $[P_{4444}]Br$ + cholinium-based ILs effectively depleted IgG and HSA at the interphase (DE_{IgG} = 100% and DE_{HSA} = 100%), regardless of the specific structure of the cholinium-based IL. Considering the remaining phosphonium-based ILs, the IL–IL-ABS composed of $[P_{i(444)1}][TsO]$ + $[Ch][H_2PO_4]$ completely removed IgG at the interphase (DE_{IgG} = 100%), followed by $[P_{4441}][CH_3SO_4]$ + $[Ch][H_2PO_4]$ (91%) > $[P_{4444}]Cl$ + $[Ch][H_2PO_4]$ (86%) > $[P_{4442}][Et_2PO_4]$ + $[Ch][H_2PO_4]$ (67%). Regarding their ability to deplete HSA at the interphase, IL–IL-ABS can be ranked as follows: $[P_{4441}][CH_3SO_4]$ + $[Ch][H_2PO_4]$ (75%) > $[P_{i(444)1}][TsO]$ + $[Ch][H_2PO_4]$ (69%) > $[P_{4444}]Cl$ + $[Ch][H_2PO_4]$ (37%) > $[P_{4442}][Et_2PO_4]$ + $[Ch][H_2PO_4]$ (30%). In all IL–IL-ABS with depletion efficiencies below 100%, the remaining proteins were mostly recovered in the top phase.

The differences in depletion efficiencies obtained can be attributed to the unique characteristics and interactions between the ILs and the proteins in each ABS. Factors such as the hydrophobicity of the phosphonium-based ILs, salting-out effects of the cholinium-based ILs, and protein size can influence the distribution and subsequent depletion/precipitation of high-abundance serum proteins.[39,40] $[P_{4444}]Br$ represents the most hydrophobic IL, exhibiting the highest depletion efficiencies, irrespective of the structure of the cholinium-based IL. The nature of the phosphonium-based IL plays a more significant role in depletion compared to the cholinium-based ILs, which primarily act as the salting-out agent. On the other hand, ILs presenting higher tendency for

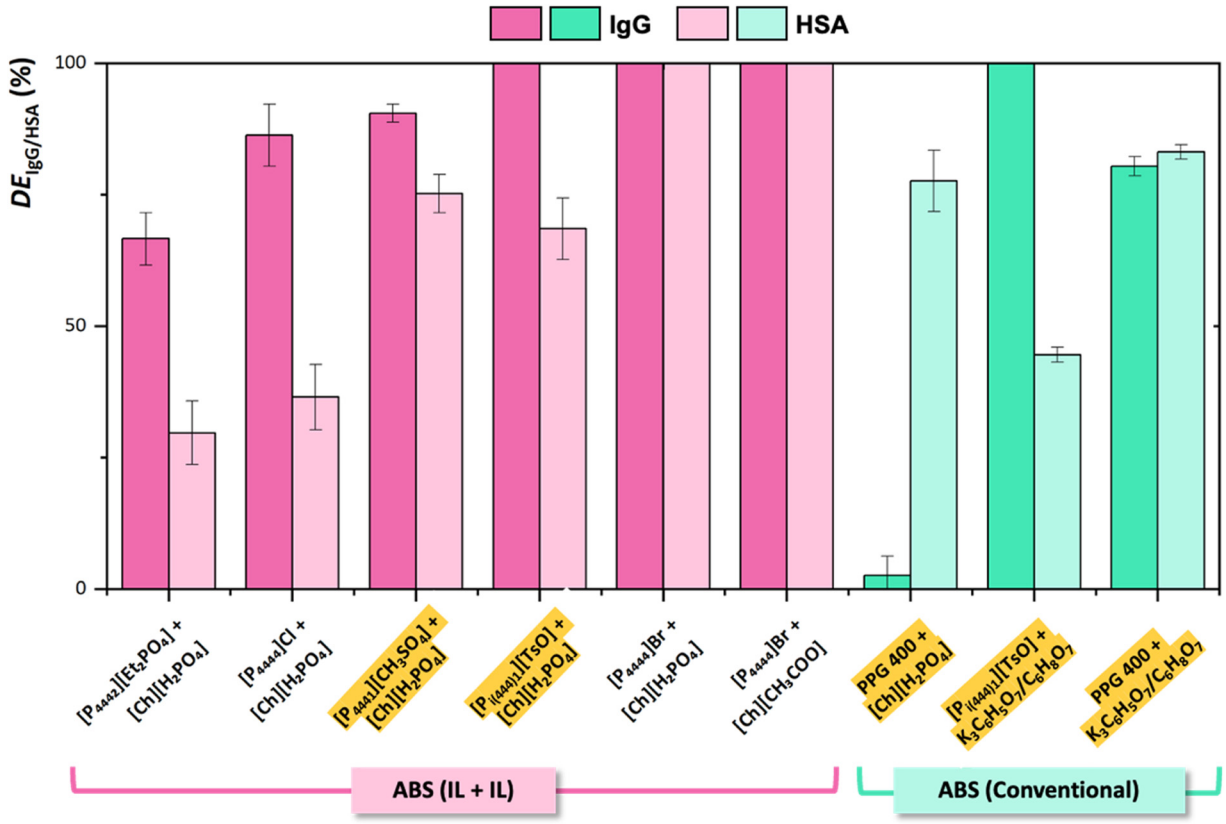

Fig. 3 Depletion efficiencies of IgG (DE_{IgG}, %) and HSA (DE_{HSA}, %) obtained for IL–IL-ABS (pink) composed of 30 or 40 wt% phosphonium-based IL + 35 wt% cholinium-based IL + 33 or 23 wt% PBS + 2 wt% human serum, and for conventional ABS (green) composed of 30 wt% $[P_{i(444)1}][TsO]$ or PPG 400 + 35 wt% $[Ch][H_2PO_4]$ or $K_3C_6H_5O_7/C_6H_8O_7$ + 33 wt% phosphate buffered saline solution (PBS) + 2 wt% human serum. Within each ABS type, darker bars correspond to IgG and lighter bars to HSA. The systems selected for subsequent HER2 extraction experiments are highlighted in yellow. Error bars represent standard deviation (n = 3).

hydration, such as $[P_{4444}]Cl$ and $[P_{4442}][Et_2PO_4]$, displayed lower efficiencies in the depletion of IgG and HSA. Overall, ILs with more hydrophobic structures tend to decrease the solubility of both IgG and HSA in the ABS aqueous phase, promoting their precipitation at the interphase. Furthermore, the depletion efficiencies of IgG were found to be higher than those of HSA in most IL–IL-ABS. This phenomenon can be explained by the relationship between the protein molecular weight and its behaviour in the system.[41] Proteins with higher molecular weights, such as IgG (150 kDa),[42] generally have reduced solubility and lower partition coefficients, rendering them more susceptible to precipitation compared to proteins with smaller molecular weights, such as HSA (65 kDa).[43]

For benchmarking and to attest IL–IL-ABS utility, conventional polymer–salt, IL–salt, and polymer–IL-ABS were also investigated. These systems were prepared using citrate buffer ($K_3C_6H_5O_7/C_6H_8O_7$) at pH 7 with either PPG 400 or $[P_{i(444)1}][TsO]$, and PPG 400 with $[Ch][H_2PO_4]$, to evaluate the role of $[Ch][H_2PO_4]$ as a salting-out agent. These pairings ensure at least one common component across the different ABS categories (polymer–salt, IL–salt, polymer–IL and IL–IL), enabling a direct and consistent comparison.

The IL–salt-ABS successfully depleted IgG at the interphase (DE_{IgG} = 100%), whereas HSA was preferentially retained in the top phase (DE_{HSA} = 39%). Compared to $[P_{i(444)1}][TsO]$ + $[Ch][H_2PO_4]$ (DE_{HSA} = 69%), it is possible to infer that the use of a second IL as the salting-out agent plays a determinant role in the removal of HSA at the interphase. Polymer–IL and polymer–salt-ABS resulted in the depletion of 3% and 80% of IgG, and 78% and 83% of HSA, respectively. While polymer–IL-ABS was surpassed by all the IL–IL-ABS in the removal of IgG at the interphase, it displayed lower to equivalent ability to deplete HSA. In the polymer–salt-ABS, the similarity between the depletion efficiency of both proteins indicates that protein molecular weight might not significantly influence protein precipitation at the interphase. In this particular type of ABS, protein precipitation at the interphase seems predominantly governed by the volume exclusion effect or reduced protein solubility in the PPG 400-rich phase, compensated by the salting-out effect of $K_3C_6H_5O_7/C_6H_8O_7$.[44] In the polymer–IL-ABS, IgG preferentially accumulates in the IL-rich bottom phase, a peculiar behaviour likely driven by specific interactions between $[Ch][H_2PO_4]$ and IgG. These results strongly suggest that the use of IL–IL-ABS has significant benefits in the

depletion process compared to conventional ABS configurations.

Upon demonstrating its capacity to effectively deplete IgG and HSA, the best performing IL–IL-ABS, namely $[P_{4444}]Br$ + $[Ch][CH_3COO]$, $[P_{4444}]Br$ + $[Ch][H_2PO_4]$, $[P_{i(444)1}][TsO]$ + $[Ch][H_2PO_4]$, and $[P_{4441}][CH_3SO_4]$ + $[Ch][H_2PO_4]$ were selected to appraise the extraction of HER2 from human serum. By employing the same conditions as in the depletion studies, the partition of HER2 was firstly analysed in ABS containing 2 wt% aqueous solution of HER2 at 15 ng mL^{-1} (*i.e.*, without serum). HER2 recovery yields were determined in the top phase of the ABS to evaluate potential losses, which must be minimized to ensure the clinical applicability of the method. The corresponding data can be found in Table S2 in the SI.

In ABS containing $[P_{i(444)1}][TsO]$ + $[Ch][H_2PO_4]$, $[P_{4441}][CH_3SO_4]$ + $[Ch][H_2PO_4]$, $[P_{i(444)1}][TsO]$ + $K_3C_6H_5O_7/C_6H_8O_7$, and PPG 400 + $K_3C_6H_5O_7/C_6H_8O_7$, HER2 selectively partitioned to the top phase, with no significant losses ($RY_{HER2} \geq 95\%$). On the contrary, HER2 was completely lost in either IL–IL-ABS formulated with $[P_{4444}]Br$. The mechanism underlying the partition of HER2 in IL–IL-ABS could be associated with the more hydrophilic environment in the $[P_{i(444)1}][TsO]$ or $[P_{4441}][CH_3SO_4]$-based ABS, which increases the solubility of HER2 in the top phase, compared to the $[P_{4444}]Br$-based ABS. These findings disclose the migration profile of HER2 before human serum introduction, where the sample matrix composition may also play a part.

Finally, the extraction of HER2 was studied in ABS containing 2 wt% HER2 spiked serum samples at concentrations that would be encountered in clinical settings (15 ng mL^{-1}).[36] Fig. 4 presents the recovery yields of HER2 obtained for the top phase and the interphase, and detailed data is provided in Table S3 in the SI. For all ABS, no HER2 was quantified in the bottom phase.

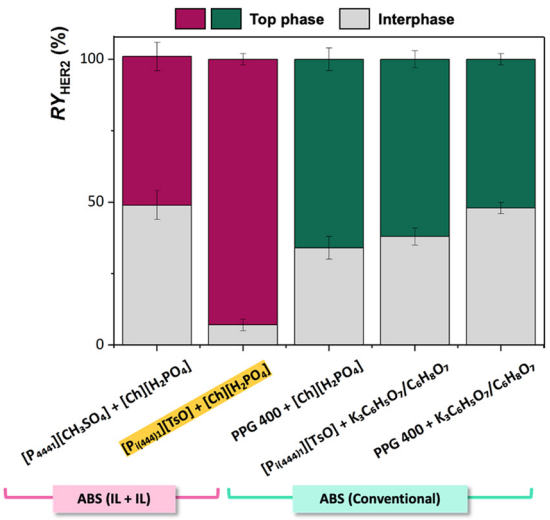

Fig. 4 Recovery yields of HER2 (RY_{HER2}, %) in IL–IL-ABS (pink) composed of 30 wt% phosphonium-based IL + 35 wt% cholinium-based IL + 33 wt% PBS + 2 wt% HER2 spiked human serum (15 ng mL^{-1}), and of conventional ABS (green) composed of 30 wt% $[P_{i(444)1}][TsO]$ or PPG 400 + 35 wt% $[Ch][H_2PO_4]$ or $K_3C_6H_5O_7/C_6H_8O_7$ + 33 wt% PBS + 2 wt% HER2 spiked human serum (15 ng mL^{-1}). Each bar is stacked to indicate the fraction of HER2 recovered in the top phase (coloured segment) and interphase (grey segment). The best-performing system for HER2 extraction is highlighted in yellow. Error bars represent standard deviation (n = 3).

Due to the presence of serum, some noteworthy differences in HER2 distribution were observed. Most ABS studied induced HER2 losses by co-precipitation at the interphase (34–49%). Although molecular weight is often associated with protein precipitation in ABS, protein concentration and solubility under the applied conditions also play a decisive role. Despite its higher molecular weight than IgG (150 kDa)[42] and HSA (65 kDa),[43] HER2 (185 kDa)[4] is present at trace levels and remains comparatively more soluble in most systems, which may contribute to reduced losses to the interphase ($RY_{HER2} \leq 49\%$). Remarkably, the ABS containing $[P_{i(444)1}][TsO]$ + $[Ch][H_2PO_4]$ exhibited the highest recovery yield of HER2 in the top phase (RY_{HER2} = 93%), with minimal losses, while achieving depletion levels of HSA and IgG at 69% and 100%, respectively. This IL–IL-ABS grants superior human serum pretreatment, providing a promising approach to enhance downstream bioanalysis.

Because sample volume directly affects multiple aspects of bioanalysis, including patient comfort, PoC implementation, retesting capacity and analytical sensitivity, the influence of serum content in ABS was systematically evaluated. Serum mass fractions between 2 and 10 wt% were studied, corresponding to sample volumes of approximately 20–100 µL per assay (estimated from the total system mass using an aqueous density approximation). This range was chosen to reduce patient burden compared to conventional clinical analyses,[45] which is particularly relevant for vulnerable populations such as cancer patients, while remaining compatible with PoC operation.[46] Under these conditions, the workflow enables straightforward handling and operational robustness, with minimal biological sample consumption in line with sustainability principles.[26] Fig. 5 presents the depletion of high-abundance proteins and the recovery of HER2 as a function of increasing serum content. Detailed results are given in the SI (Table S4).

Fig. 5A demonstrates that the depletion efficiency of IgG remained consistent at 100% across all serum mass fractions tested. In turn, the depletion efficiency of HSA improved with increasing serum content, rising from 69% at 2 wt% serum to 74% at 5 wt% and 84% at 10 wt% serum. At higher protein concentrations, phenomena such as protein aggregation, macromolecular crowding, and reduced solvation likely promote increased protein–protein interactions, ultimately leading to precipitation.[47] More significantly, Fig. 5B highlights the system's ability to maintain HER2 recovery yield in the top phase as serum mass fraction increases from 2 wt% to 10 wt%, without phase saturation. The use of higher serum contents may enhance the sensitivity of detection assays, enabling a broader dynamic range in HER2 quantification without substantially increasing sample volume requirements, costs and resource consumption.

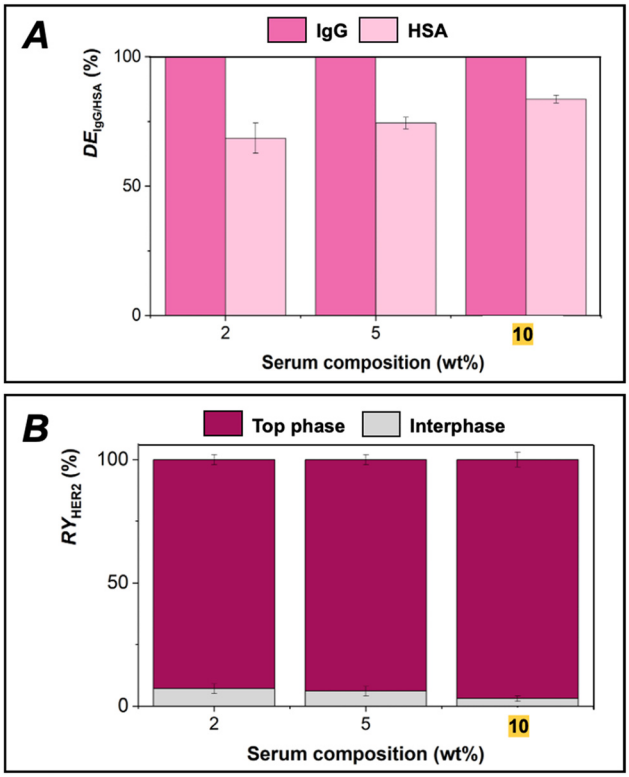

Fig. 5 Effect of serum composition on protein separation in ABS composed of 30 wt% $[P_{i(444)1}][TsO]$ + 35 wt% $[Ch][H_2PO_4]$ + 33/30/25 wt% PBS + 2/5/10 wt% human serum: (A) depletion efficiencies of IgG (DE_{IgG}, %) and HSA (DE_{HSA}, %), with darker pink bars representing IgG and lighter pink bars representing HSA; (B) recovery yields of HER2 (RY_{HER2}, %) shown as stacked bars, with the pink segment representing the top phase and the grey segment representing the interphase. The best-performing conditions are highlighted in yellow. Error bars represent standard deviation (n = 3).

These optimized conditions will support the development of a microfluidic platform designed to improve HER2 quantification sensitivity.

HER2 detection in microfluidic devices

To develop a sensitive and specific detection method for detecting HER2 in human serum, a microfluidic device using a sandwich immunoassay format with protein G beads as the solid support was designed (Fig. 6). The experimental design progressed from an ideal buffer system to a more complex biological matrix. Initially, the assay's performance was tested in PBS, followed by experiments using spiked human serum samples. This stepwise approach allowed to evaluate the impact of matrix effects on the assay performance.

As depicted in Fig. 6A, the microfluidic device employed protein G-coated beads to immobilize anti-HER2 capture antibodies, ensuring oriented antibody presentation for optimal antigen binding. This design provides advantages such as increased surface area and improved mass transfer kinetics, which can potentially enhance the assay's sensitivity and efficiency.[35] For detection, antibodies labelled with ALEXA 430, a bright and photostable fluorophore, were used. This labelling strategy, combined with fluorescence microscopy using an appropriate excitation source and filter set, made possible sensitive and specific detection of HER2.

To assess the assay's performance, fluorescence intensities obtained in PBS or undiluted human serum at two key concentrations were compared: 25 ng mL^{-1} of HER2 (positive control) and 0 ng mL^{-1} (negative control). Fig. 6B shows the assay's ability to distinguish between HER2-positive and HER2-negative samples in different matrices, while detailed information is given in the SI (Table S5). The effectiveness of the developed approach was quantitatively evaluated by calculating the signal ratios between the positive and negative controls. By systematically comparing the assay's performance in PBS and human serum, the challenges presented by complex biological matrices were identified, leading to the development of strategies to optimize HER2 detection under clinically relevant conditions.

In PBS, a signal ratio of 2 between the positive control (25 ng mL^{-1} HER2) and the negative control was observed. This two-fold increase in fluorescence intensity indicates a clear distinction between HER2-positive and HER2-negative samples in an ideal buffer system. The robust signal-to-background ratio in PBS demonstrates the effectiveness of the assay design proposed, encompassing efficient capture antibody immobilization on protein G beads, specific HER2 binding, and sensitive detection using ALEXA 430-labeled antibodies. In the case of human serum samples, a decrease in the signal ratio to 1.3 between the positive control and the negative control was observed. The reduction in signal-to-background ratio is expected due to the complex nature of serum samples.[48] This can be due to several factors, including matrix effects from interfering serum proteins, background autofluorescence from serum components, and molecular crowding affecting antibody–antigen binding kinetics.[49,50]

Despite these challenges, the assay maintained its ability to distinguish between HER2-positive and HER2-negative samples in serum, albeit with reduced sensitivity compared to PBS. The difference in signal ratios between PBS and serum gives valuable insights into the assay's performance in different sample matrices, demonstrating the robustness of the microfluidic platform and enabling the quantification of serum matrix effects. The assay's ability to distinguish HER2-positive samples suggests its potential for clinical applications, highlighting its relevance in complex biological samples.

HER2 detection *via* IL–IL-ABS integration with microfluidic platforms

To address the reduced signal ratio in serum samples, several strategies could be explored, including optimizing blocking agents to reduce non-specific binding and introducing sample pretreatment methods to remove interfering serum components.[51,52] Additionally, investigating signal

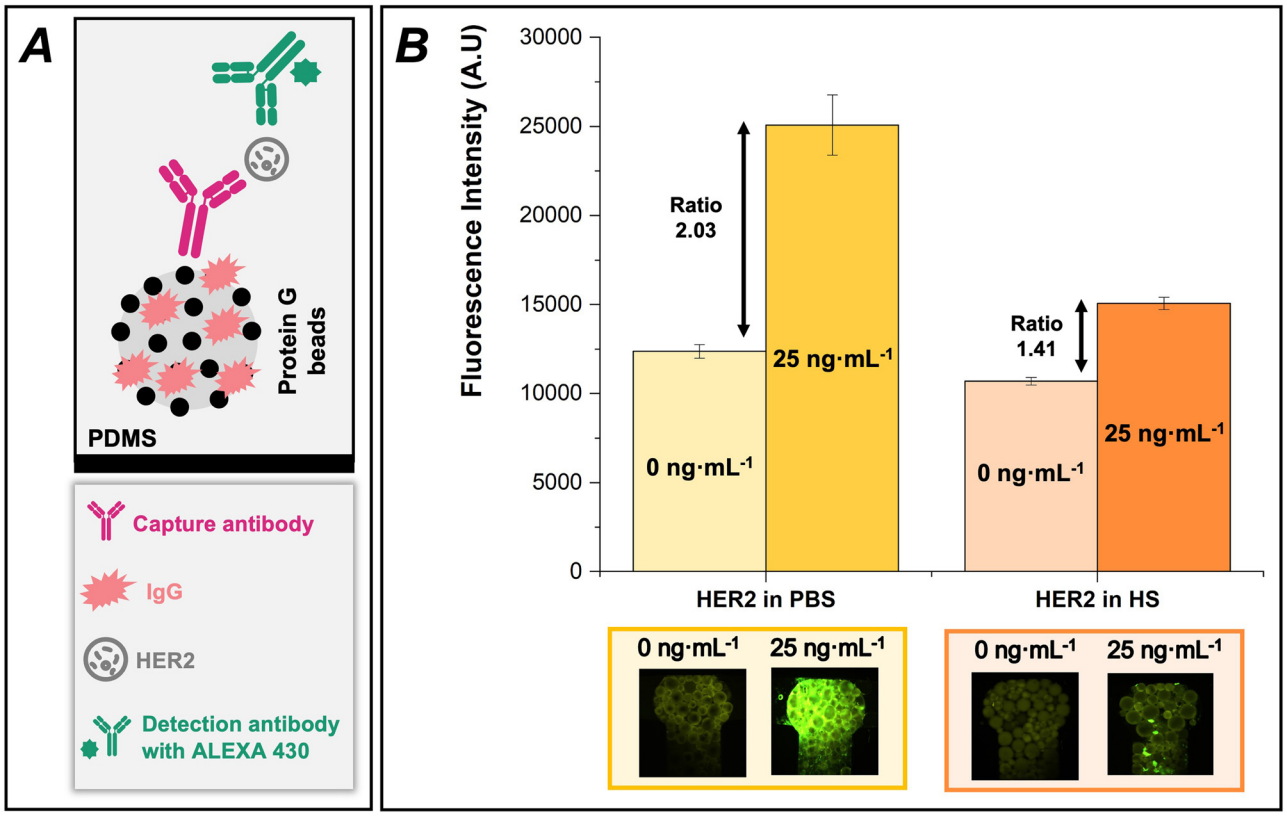

Fig. 6 HER2 detection in a microfluidic device. (A) Microbead-based sandwich immunoassay implemented on the microfluidic platform. (B) Fluorescence intensity measurements in PBS (yellow) and human serum (HS, orange), with lighter bars representing 0 ng mL^{-1} and darker bars representing 25 ng mL^{-1} HER2. Corresponding fluorescence images are shown below each condition. Error bars represent standard deviation (n = 3).

amplification techniques, such as enzymatic or nanoparticle-based approaches, could enhance detection sensitivity in serum.[53,54] Instead, this work integrates an innovative pretreatment step using IL–IL-ABS before microfluidic detection (Fig. 7).

The analytical workflow consists of two integrated steps, as illustrated in Fig. 7A. First, the ABS composed of $[P_{i(444)1}][TsO]$ + $[Ch][H_2PO_4]$, which comprises two ILs that work synergistically to selectively precipitate IgG and HSA at the interphase while simultaneously extracting HER2 into a distinct phase. Second, a microfluidic immunoassay for HER2 detection following extraction. The biomarker-enriched top phase is analysed using the microbead-based sandwich immunoassay within a microfluidic chip, allowing for sensitive and specific detection through fluorescence-based readout, even at low concentrations. Furthermore, a final ABS mass of 1 g was established as an ideal target to minimize serum and reagent consumption, while ensuring seamless off-chip integration with microfluidic detection, suitable for PoC use.

Fig. 7B presents the key performance metrics of the HER2 detection assay across various sample matrices, namely the sensitivity curves, LoDs and the data correlation (R^2) with dose–response fitting. The fluorescence intensity is plotted against HER2 concentration for four different conditions: HER2 in PBS, HER2 in untreated human serum, HER2 spiked in the top phase of the ABS, and HER2 in the top phase of the ABS after serum pretreatment. Detailed data and signal ratios obtained for each condition are provided in the SI (Table S5).

The signal ratio between 25 ng mL^{-1} HER2 and the negative control clarifies the assay's dynamic range and sensitivity. Signal ratios of 2.03, 1.41, 2.12, and 1.47 were obtained for PBS, untreated human serum, ABS top phase (without serum), and ABS top phase after serum pretreatment, respectively. The data correlation values, all above 0.98, demonstrate excellent dose–response fitting across all conditions, attesting assay's reliability and precision, which is further supported by low RSD (%) values (3–12%) observed across the tested concentration range. The LoDs further quantify the assay's sensitivity in each matrix. The LoD for HER2 in PBS was 18.99 ng mL^{-1}, increasing to 24.33 ng mL^{-1} in untreated human serum, thus confirming the detrimental impact of matrix effects when analysing complex biological samples. Spiking HER2 directly into the top phase of the ABS (without serum) resulted in an improved LoD of 15.52 ng mL^{-1} compared to direct serum analysis, attesting the high compatibility between the IL-based medium and the developed microfluidic immunoassay. The lowest LoD of 14.06 ng mL^{-1}, achieved in the ABS top

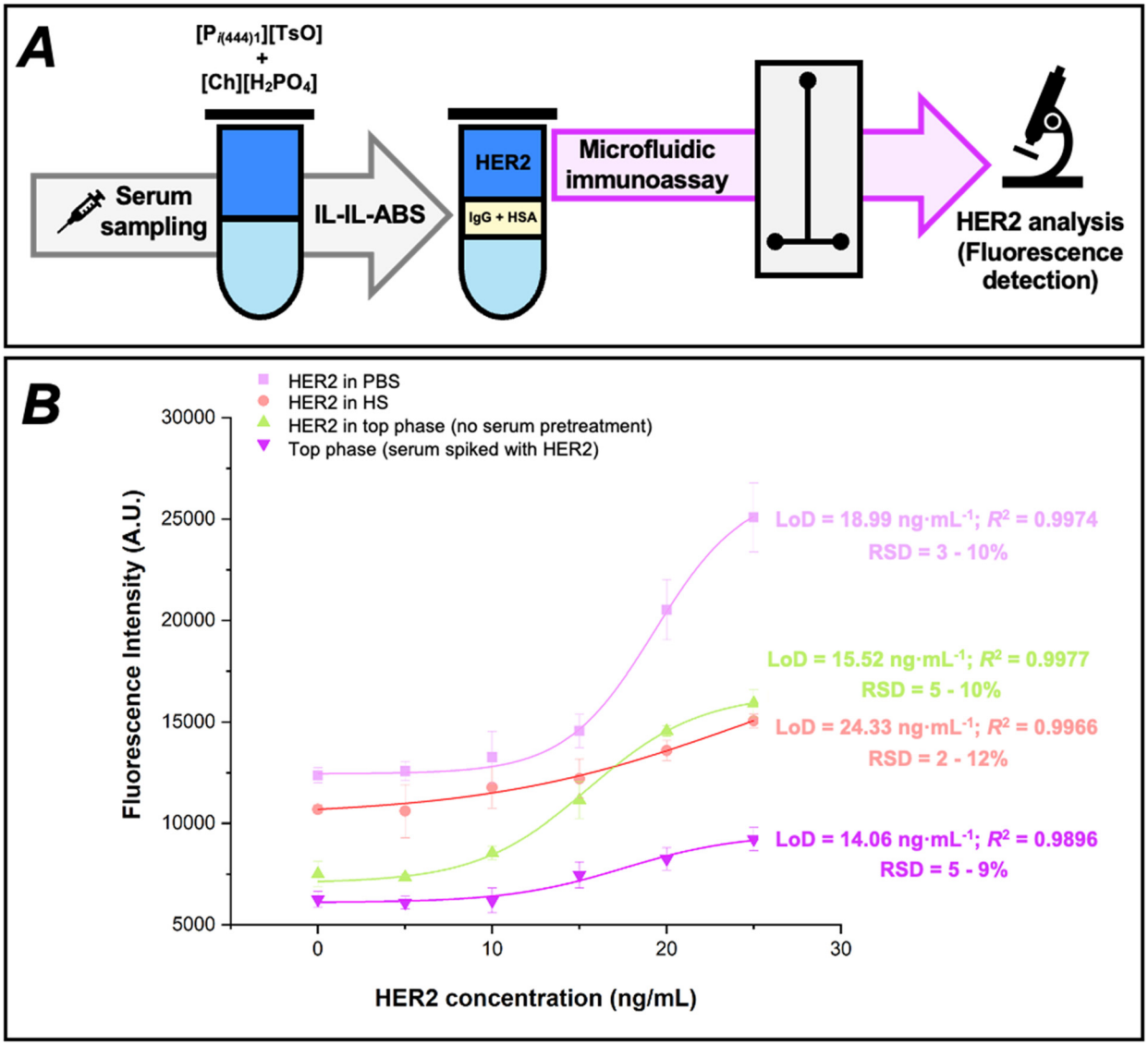

Fig. 7 Analytical strategy and performance evaluation of the developed HER2 detection assay. (A) Integrated analytical workflow, highlighting the sequential steps from sample pretreatment using IL–IL-ABS to microfluidic-based HER2 detection. (B) Performance metrics of the assay across different matrices, including sensitivity curves, LoDs and RSD (%) values for HER2 in PBS (pink squares), untreated serum (red circles), the spiked ABS top phase without serum (green triangles), and the ABS top phase after serum pretreatment (purple inverted triangles). Solid lines represent the best-fit curves for each condition. Error bars indicate standard deviation (n = 3).

phase after serum pretreatment, represents a 42% improvement over untreated serum and even surpasses the sensitivity in PBS. Despite its protein-free nature, PBS exhibited higher background noise than IL–IL-ABS pretreated serum, indicating suboptimal conditions for antibody–antigen interactions under the applied assay conditions.[35] Nevertheless, PBS displays a higher fold increase in fluorescence intensity with increasing HER2 concentration (signal ratio = 2.03), which originates from a steeper concentration-dependent signal amplification rather than improved analytical sensitivity. In this case, the larger signal gain outweighs the elevated baseline, leading to a higher ratio despite poorer background control. HER2 sensitivity is significantly enhanced after pretreatment due to the selective depletion of IgG and HSA, which reduces matrix effects and background, and the stabilizing effect of the IL-containing phase. This leads to a lower LoD, despite a more moderate signal amplification compared to PBS.

Compared to previously reported microfluidic approaches for HER2 detection, the proposed assay provides competitive sensitivity, particularly considering its higher degree of simplicity.[55,56] Many of the most sensitive platforms described to date rely on advanced nanomaterials or elaborated signal amplification strategies, which often increase fabrication complexity, cost and the need for extensive surface modifications.[15,16,18,19] In contrast, the present assay achieves a clinically relevant LoD of 14.06 ng mL^{-1}, combining moderate sensitivity with operational

simplicity and robust compatibility with complex biological matrices. Overall, the proposed approach represents an accessible alternative to more technically demanding biosensors, with integration of portable readout systems representing a key step for future development.

The distinctive advantage of the proposed assay lies in the IL–IL-ABS pretreatment step, which mitigates matrix interferences to which microfluidic immunoassays are particularly susceptible, enhancing analytical performance. The device requires only limited manual handling and small sample volumes, making it suitable for PoC and resource-limited settings, where conventional assays such as ELISA are often impractical due to reliance on centralized laboratories and skilled personnel. Economically, the assay consumes low amounts of reagents and is amenable to integration with low-cost, portable detection platforms, with fluorescence imaging employed here serving solely as a proof-of-concept. Although microfluidic device fabrication is an upstream technical consideration, it does not impact end-user operation, as devices would be supplied as ready-to-use disposable cartridges. While not yet fully automated, this workflow demonstrates a clear pathway toward PoC translation and near-patient testing in rural and underserved regions.

Finally, this work was performed using commercially available human serum for reasons of technology development and reproducibility. While the selective depletion of IgG and HSA demonstrates the platform's effectiveness in mitigating matrix effects, patient-to-patient variability, arising from differences in physiological conditions, disease states, and comorbidities, may influence assay performance in clinical samples. Future work should therefore focus on validating the IL–IL-ABS microfluidic platform with patient-derived samples.

Conclusions

This work reports the successful development and optimization of a new method for HER2 detection in complex biological matrices, integrating an innovative pretreatment step prior to microfluidic detection. The IL–IL-ABS pretreatment combines high selectivity, biomarker-friendly extraction conditions, and operational simplicity. By employing two tailored ILs, it allows the selective depletion of high-abundance proteins while efficiently extracting HER2 into distinct phases. The all-aqueous conditions preserve HER2 integrity, minimizing the risk of false negatives in clinical testing. Additionally, this approach eliminates multi-step procedures, organic solvents, and costly reagents, offering economic and environmental benefits. The IL–IL-ABS enabled complete depletion of IgG and 84% removal of HSA at the interphase, while ensuring a high HER2 recovery yield (97%), overcoming the limitations of previous methods that often led to substantial biomarker losses.

The IL–IL-ABS pretreatment strategy significantly enhanced the analytical performance of the microfluidic immunoassay in human serum samples, confirming its suitability for clinical and PoC applications. A lower LoD of 14.06 ng mL^{-1} was achieved in pretreated serum, outperforming both untreated serum (24.33 ng mL^{-1}) and even the ideal PBS matrix (18.99 ng mL^{-1}). This improvement reflects the effective removal of high-abundance proteins by the $[P_{i(444)1}][TsO]$ + $[Ch][H_2PO_4]$ ABS, which substantially reduced matrix effects and enabled more reliable biomarker quantification.

Overall, a significant step forward in HER2 detection methodologies is achieved, combining innovative sample pretreatment with a sensitive microfluidic platform that provides fast response times at clinical sensitivities. The enhanced performance in complex biological matrices paves the way for more accurate and reliable HER2 quantification in both clinical and decentralized settings, offering a promising tool to improve breast cancer diagnosis and monitoring at the PoC.

Author contributions

M. S. M. M.: methodology, validation, formal analysis, investigation, data curation, writing – original draft, visualization; I. A.: investigation, data curation; M. C. S.: investigation, data curation; V. C.: conceptualization, writing – review & editing; M. G. F.: conceptualization, funding acquisition, supervision, writing – review & editing; F. A. eS.: conceptualization, writing – review & editing, supervision, funding acquisition, project administration; J. P. C.: conceptualization, funding acquisition, supervision, writing – review & editing.

Conflicts of interest

There are no conflicts to declare.

Data availability

The data supporting this article have been included as part of the supplementary information (SI).

Supplementary information: detailed experimental data regarding depletion efficiencies of IgG and HSA, recovery yields of HER2 and fluorescence intensity measurements of HER2 in microfluidic devices. See DOI: https://doi.org/10.1039/d5lc01010a

Acknowledgements

This work was developed within the scope of the project CICECO Aveiro Institute of Materials, UID/50011/2025 (DOI: https://doi.org/10.54499/UID/50011/2025) & LA/P/0006/2020 (DOI: https://doi.org/10.54499/LA/P/0006/2020), financed by national funds through the FCT/MCTES (PIDDAC). INESC MN acknowledges pluriannual financing from FCT through UID/PRR/5367/2025 and UID/5367/2025. This work was developed within the project ILSurvive, PTDC/EMD-TLM/3253/2020 (DOI: https://doi.org/10.54499/PTDC/EMD-TLM/3253/2020), funded

by national funds (OE), through FCT/MCTES. M. S. M. M. acknowledges FCT for the doctoral grant 2022.11229.BD (DOI: https://doi.org/10.54499/2022.11229.BD). F. A. eS. acknowledges FCT for the researcher contract CEECIND/03076/2018/CP1559/CT0024 (DOI: https://doi.org/10.54499/CEECIND/03076/2018/CP1559/CT0024) under the Scientific Employment Stimulus – Individual Call 2018.

References

1 F. Bray, M. Laversanne, H. Sung, J. Ferlay, R. L. Siegel, I. Soerjomataram and A. Jemal, *Ca-Cancer J. Clin.*, 2024, **74**, 229–263.
2 L. Wu and X. Qu, *Chem. Soc. Rev.*, 2015, **44**, 2963–2997.
3 P. Gamble, R. Jaroensri, H. Wang, F. Tan, M. Moran, T. Brown, I. Flament-Auvigne, E. A. Rakha, M. Toss, D. J. Dabbs, P. Regitnig, N. Olson, J. H. Wren, C. Robinson, G. S. Corrado, L. H. Peng, Y. Liu, C. H. Mermel, D. F. Steiner and P.-H. C. Chen, *Commun. Med.*, 2021, **1**, 14.
4 N. Iqbal and N. Iqbal, *Mol. Biol. Int.*, 2014, **2014**, 1–9.
5 S. Ahn, J. W. Woo, K. Lee and S. Y. Park, *J. Pathol. Transl. Med.*, 2020, **54**, 34–44.
6 C. Lottner, S. Schwarz, S. Diermeier, A. Hartmann, R. Knuechel, F. Hofstaedter and G. Brockhoff, *J. Pathol.*, 2005, **205**, 577–584.
7 J. T. Gohring, P. S. Dale and X. Fan, *Sens. Actuators, B*, 2010, **146**, 226–230.
8 C. B. Moelans, R. A. de Weger, E. Van der Wall and P. J. van Diest, *Crit. Rev. Oncol. Hematol.*, 2011, **80**, 380–392.
9 B. Leyland-Jones and B. R. Smith, *Lancet Oncol.*, 2011, **12**, 286–295.
10 L. Lam, N. McAndrew, M. Yee, T. Fu, J. C. Tchou and H. Zhang, *Biochim. Biophys. Acta*, 2012, **1826**, 199–208.
11 J. P. Monteiro, S. M. Predabon, E. G. Bonafé, A. F. Martins, A. G. Brolo, E. Radovanovic and E. M. Girotto, *J. Nanotechnol.*, 2017, **28**, 045206.
12 L. Loo, J. A. Capobianco, W. Wu, X. Gao, W. Y. Shih, W. H. Shih, K. Pourrezaei, M. K. Robinson and G. P. Adams, *Anal. Chem.*, 2011, **83**, 3392–3397.
13 H. Tavakoli, S. Mohammadi, X. Li, G. Fu and X. Li, *TrAC, Trends Anal. Chem.*, 2022, **157**, 116806.
14 G. Fu, W. Zhou and X. Li, *Lab Chip*, 2020, **20**, 2218–2227.
15 M. Shamsipur, M. Emami, L. Farzin and R. Saber, *Biosens. Bioelectron.*, 2018, **103**, 54–61.
16 L. Loo, J. A. Capobianco, W. Wu, X. Gao, W. Y. Shih, W.-H. Shih, K. Pourrezaei, M. K. Robinson and G. P. Adams, *Anal. Chem.*, 2011, **83**, 3392–3397.
17 J. T. Gohring, P. S. Dale and X. Fan, *Sens. Actuators, B*, 2010, **146**, 226–230.
18 S. Carvajal, S. N. Fera, A. L. Jones, T. A. Baldo, I. M. Mosa, J. F. Rusling and C. E. Krause, *Biosens. Bioelectron.*, 2018, **104**, 158–162.
19 J. V. Jokerst, A. Raamanathan, N. Christodoulides, P. N. Floriano, A. A. Pollard, G. W. Simmons, J. Wong, C. Gage, W. B. Furmaga, S. W. Redding and J. T. McDevitt, *Biosens. Bioelectron.*, 2009, **24**, 3622–3629.
20 R. C. B. Marques, S. Viswanathan, H. P. A. Nouws, C. Delerue-Matos and M. B. González-García, *Talanta*, 2014, **129**, 594–599.
21 K. C. Chan, D. A. Lucas, D. Hise, C. F. Schaefer, Z. Xiao, G. M. Janini, K. H. Buetow, H. J. Issaq, T. D. Veenstra and T. P. Conrads, *Clin. Proteomics*, 2004, **1**, 101–225.
22 G. Vidarsson, G. Dekkers and T. Rispens, *Front. Immunol.*, 2014, **5**, 520.
23 H. J. Issaq, Z. Xiao and T. D. Veenstra, *Chem. Rev.*, 2007, **107**, 3601–3620.
24 H. J. Issaq and T. D. Veenstra, *Proteomic and Metabolomic Approaches to Biomarker Discovery*, Elsevier, Amsterdam, 2020, pp. 95–102.
25 V. Polaskova, A. Kapur, A. Khan, M. P. Molloy and M. S. Baker, *Electrophoresis*, 2010, **31**, 471–482.
26 Á. I. López-Lorente, F. Pena-Pereira, S. Pedersen-Bjergaard, V. G. Zuin, S. A. Ozkan and E. Psillakis, *TrAC, Trends Anal. Chem.*, 2022, **148**, 116530.
27 M. S. M. Mendes, M. E. Rosa, F. Ramalho, M. G. Freire and F. A. e. Silva, *Sep. Purif. Technol.*, 2023, **317**, 123875.
28 F. D. Raymond, D. W. Moss and D. Fisher, *Clin. Chim. Acta*, 1994, **227**, 111–120.
29 M. A. O. da Silva and M. A. Z. Arruda, *Talanta*, 2009, **77**, 985–990.
30 M. S. M. Mendes, M. E. Rosa, J. A. P. Coutinho, M. G. Freire and F. A. e. Silva, *Int. J. Biol. Macromol.*, 2023, **253**, 127540.
31 J. Kim, H. Shin, J. Kim, J. Kim and J. Park, *PLoS One*, 2015, **10**, 1–16.
32 Z. Du, Y. L. Yu and J. H. Wang, *Chem. – Eur. J.*, 2007, **13**, 2130–2137.
33 M. F. Yee, G. N. Emmel, E. J. Yang, E. Lee, J. H. Paek, B. M. Wu and D. T. Kamei, *Front. Chem.*, 2018, **6**, 1–10.
34 M. E. Rosa, M. S. M. Mendes, E. Carmo, J. P. Conde, J. A. P. Coutinho, M. G. Freire and F. A. e. Silva, *Sep. Purif. Technol.*, 2023, **322**, 124248.
35 F. C. Flora, S. B. Relvas, F. A. e. Silva, M. G. Freire, V. Chu and J. P. Conde, *Biosensors*, 2023, **13**, 334.
36 A. Shamshirian, A. R. Aref, G. W. Yip, M. E. Warkiani, K. Heydari, S. Razavi Bazaz, Z. Hamzehgardeshi, D. Shamshirian, M. Moosazadeh and R. Alizadeh-Navaei, *BMC Cancer*, 2020, **20**, 1049.
37 M. S. M. Mendes, V. Chu, M. G. Freire, F. A. e. Silva and J. P. Conde, *Anal. Chim. Acta*, 2026, **1385**, 345001.
38 R. R. G. Soares, P. Novo, A. M. Azevedo, P. Fernandes, M. R. Aires-Barros, V. Chu and J. P. Conde, *Lab Chip*, 2014, **14**, 4284–4294.
39 J. A. Asenjo and B. A. Andrews, *J. Chromatogr. A*, 2011, **1218**, 8826–8835.
40 B. A. Andrews, A. S. Schmidt and J. A. Asenjo, *Biotechnol. Bioeng.*, 2005, **90**, 380–390.
41 P. Wingfield, *Curr. Protoc. Protein Sci.*, 1998, **13**, A.3F.1–A.3F.8.
42 D. Prozeller, C. Rosenauer, S. Morsbach and K. Landfester, *Biointerphases*, 2020, **15**, 031009.
43 R. Raoufinia, A. Mota, N. Keyhanvar, F. Safari, S. Shamekhi and J. Abdolalizadeh, *Adv. Pharm. Bull.*, 2016, **6**, 495–507.
44 S. Raja, V. R. Murty, V. Thivaharan, V. Rajasekar and V. Ramesh, *Sci. Technol.*, 2012, **1**, 7–16.

45 D. H. Chace, V. R. De Jesús and A. R. Spitzer, *Bioanalysis*, 2014, **6**, 2791–2794.
46 National Center for Biotechnology Information, *Point-of-Care Testing*, https://www.ncbi.nlm.nih.gov/books/NBK592387/, (accessed 23 January 2026).
47 R. J. Ellis and A. P. Minton, *Biol. Chem.*, 2006, **387**, 485–497.
48 J. L. Bock, *Clin. Chem.*, 2000, **36**, 628–646.
49 R. J. Ellis, *Trends Biochem. Sci.*, 2001, **26**, 597–604.
50 J. R. Lakowicz, *Principles of Fluorescence Spectroscopy*, Springer, Boston, 2006, pp. 45–78.
51 R. M. Lequin, *Clin. Chem.*, 2005, **51**, 2415–2418.
52 A. M. Azevedo, A. G. Gomes, P. A. J. Rosa, I. F. Ferreira, A. M. M. O. Pisco and M. R. Aires-Barros, *Sep. Purif. Technol.*, 2009, **65**, 14–21.
53 P. K. Jain, X. Huang, I. H. El-Sayed and M. A. El-Sayed, *Acc. Chem. Res.*, 2008, **41**, 1578–1586.
54 C. Niemeyer and C. Mirkin, *Nanobiotechnology: Concepts, Applications and Perspectives*, Wiley, Weinheim, 2004, pp. 201–235.
55 M. Freitas, H. P. A. Nouws and C. Delerue-Matos, *Electroanalysis*, 2019, **31**, 121–128.
56 K. Malecka, D. Pankratov and E. Ferapontova, *Anal. Chim. Acta*, 2019, **1077**, 140–149.